IEEE Access
Multidisciplinary | Rapid Review | Open Access Journal

Received July 13, 2020, accepted July 23, 2020, date of publication July 28, 2020, date of current version August 13, 2020.

Digital Object Identifier 10.1109/ACCESS.2020.3012486

Analytical Inverse Design of Polarization-Insensitive Photonic Filters by Tailoring Fabry-Perot Interference

CONSTANTINOS VALAGIANNOPOULOS, (Senior Member, IEEE)
Department of Physics, Nazarbayev University, Astana 010000, Kazakhstan
e-mail: konstantinos.valagiannopoulos@nu.edu.kz

This work was supported in part by the Nazarbayev University under Grant 090118FD5349 and Grant SST2017031, and in part by Ministry of Education and Science of Republic of Kazakhstan (MES RK) State-Targeted Program under Grant BR05236454.

ABSTRACT Filtering of photonic signals of a certain frequency while suppressing all the others of a specific band for both electromagnetic signal polarizations, becomes possible with a single dielectric layer by properly engineering the occurred Fabry-Perot interference. Analytical formulas for combinations of cavity size, material texture and incoming angle are given so that the filtering purpose is optimally served. In this way, inverse design for a simple class of optical setups is rigorously performed and, if the employed medium is very dense and the working band narrow enough, sharp filters with increased frequency selectivity are obtained.

INDEX TERMS Fabry-Perot interference, photonic filter, inverse design.

I. INTRODUCTION

Design of electronic filters that reject the unwanted signal frequencies while providing good transmission across the desired band, has been a traditional research and development topic for many decades during the past century. Indeed, the optimal combination of capacitors and inductors in various connections and setups constituted the objective of several standard textbooks [1]. With the advent of wave digital filtering [2], where the time delays interpreted via physical modeling principles, the performed functionalities acquired significant further potential. Given specific features for the frequency response, the old design formulas by P. Chebyshev and S. Butterworth have been refined [3] to control spurious reaction and insertion loss. Similar techniques have been extended to support filtering processes for spatially distributed two-dimensional signals [4] and their design recipes are being continuously improved [5] by incorporating additional active components.

Photonic filtering, where the electronic signals are replaced by the vectors of electromagnetic fields, is a more challenging operation requiring low loss, high bandwidth, immunity to interferences, tunability, and reconfigurability [6]. Agenda-setting contributors have proposed photonic circuits, in which beams of light redirect the flow toward specific directions [7] and parity-time symmetric bilayers exhibit extreme tunneling selectivity [8]. In addition, photonic crystals structures enabling transparency throughout the visible spectrum at one angle and filtering out all the others have been fabricated [9] while the focusing of a radially polarized field at a spot size significantly smaller than for linear polarization has been experimentally demonstrated [10]. Furthermore, spatial squeezing of light waves is recorded into nanometer-sized optical cavities [11] and integrated systems for photonic signal processing have been introduced [12]. Finally, all these enlightening theoretical ideas and practically applicable concepts have ignited substantial funding interest; indeed, large programs have been recently approved for research on wave manipulation via plasmonic interferences [13] and three-dimensional photonic filters for full duplex network links [14].

A key mechanism behind the modeling and design of such electromagnetic-field filters is the Fabry-Perot interference [15] expressing the simultaneous existence of waves propagating along various directions. It is a generic effect present in several photonic setups like maser resonators [16], nanotubes electron waveguides [17] and multiplexed fiber Bragg gratings [18]. Suitably engineered Fabry-Perot resonances have been also utilized in numerous photonic applications like photodetecting in microcavities [19], optical

The associate editor coordinating the review of this manuscript and approving it for publication was Wenjie Feng.

sensing in fibers [20], absorption in thin coatings [21] and full-color tunability of inorganic electrochromic devices [22].

Fabry-Perot interference is such a ubiquitous operation found very useful also to interactions between non-photonic waves like quantum particle beams that tunnel through potential wells [23], [24] or matter waves employed for estimating the macroscopic parameters of quantum media samples [25]. Similarly, interference of acoustic waves is exploited in ultrasonic hydrophones used for the measurement of pressure [26] and fiber-optic sensing [27]. In addition, Fabry-Perot resonances of mechanical waves appear in optical rings [28], in diaphragm sensors [29] and in pairs of vibrating membranes entanglable at their steady state [30].

The fabrication of Fabry-Perot planar resonators for photonic applications is also feasible through a variety of methods enabled by recent advances in thin film industry and technology [31]. In particular, a template-confined micro-reflow process is implemented for full-color filter arrays [32] and even lithography-free construction is possible by depositing thin layers on required substrates with low cost [33]. Moreover, micro Fabry-Perot interferometers are machined in a single-mode fiber by using a near-infrared femtosecond laser [34] while similar layered setups are grown on suitable substrates by molecular beam epitaxy [35]. It should be finally noted that interference cavities are also constructable via chemical methods involving solvothermal synthesis [36] or epoxy growing on metallic bases [37].

In this work, we consider one of the simplest members from this generic and easy-to-fabricate class of devices, namely, a single planar dielectric cavity, to build a photonic bandpass filter. The operational bandwidth and the selected frequency are given and the size of the slab, the texture of the material and the incoming angle are optimally selected to serve such a filtering purpose for both the polarizations, like in [38]. More specifically, the thicknesses of the cavity corresponding to various tailored Fabry-Perot resonance orders are analytically derived; to this end, the influence of the characteristic frequencies, the line of incidence and the permittivity of the material on the performance of the filter, is identified. Since the specifications of the transmissivity are pre-determined, this study elaborates an inverse design problem, a research direction that has recently gained substantial popularity within the broad area of Photonics. Indeed, several approaches like level-set geometric representations [39], gradient-based methods [40], deep learning algorithms [41], integral transformations [42], tight parametric sweeps [43] and topology optimizations [44], have been followed to find the best photonic structure observing a pre-specified aim. The provided analytical expressions for the inverse design of a frequency selector with extremely simple configuration, contribute to these advances and may inspire further theoretical or experimental efforts towards optimal polarization-insensitive filters.

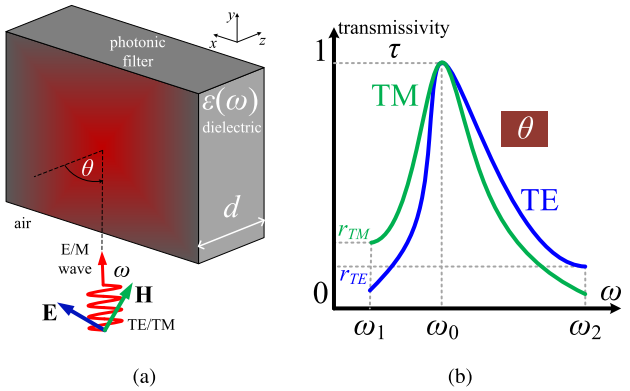

FIGURE 1. (a) The physical configuration of the considered photonic filter: a planar slab of thickness d is illuminated by an electromagnetic wave of frequency ω that meets the interface at angle θ. (b) Specifications for the inverse design of a photonic filter with 100% transmissivity $\tau_{TE/TM}$ at $\omega = \omega_0$ and no other local maximum within the frequency range $\omega_1 < \omega < \omega_2$, for both wave polarizations. The performance of the filter is judged by how much suppressed are the maximal residual transmissivities $r_{TE/TM}$ at the ends of the considered band, for a fixed angle θ.

II. MATHEMATICAL FORMULATION

We consider the structure depicted in Fig. 1(a), where a plane wave of oscillation frequency ω meets obliquely under angle θ a planar dielectric layer of thickness d. In Fig. 1(a), the used Cartesian coordinate system (x, y, z) is defined and the relative permittivity of the material filling the slab is denoted by $\varepsilon(\omega)$; the incoming illumination can be either of TE (electric field parallel to y axis) or TM (magnetic field parallel to y axis) type. The incident field $F_{y,inc} = e^{-ik(z\cos\theta + x\sin\theta)}$ is of unitary amplitude and may correspond to electric ($F_y = E_y$, TE) or magnetic ($F_y = H_y$, TM) one; the symbol $k = \omega/c$ is used for the free-space wavenumber while c is the speed of light into vacuum that surrounds the structure. Naturally, the transmitted field is expressed as: $F_{y,inc} = Te^{-ik(z\cos\theta + x\sin\theta)}$, where T is the complex transmission coefficient determinable from boundary conditions.

As indicated by Fig. 1(b), one may desires unitary transmissivity $\tau = |T|^2$ at a specific frequency $\omega = \omega_0$ and a given angle θ for both polarizations (TE/TM). In case the dielectric is dispersion-free ($\varepsilon(\omega) = \varepsilon > 1$), one of the following discrete thicknesses for the layer can be selected [45]:

$$d = \frac{n\pi c}{\omega_0\sqrt{\varepsilon - \sin^2\theta}} \equiv \frac{n\pi}{k_0 u(\theta)}, \tag{1}$$

where $k_0 = \omega_0/c$ for $n \in \mathbb{N}^*$. Under this assumption, the explicit forms for the transmissivities are given by [46]:

$$\tau_{TE} = \frac{1}{\cos^2\left(n\pi\frac{\omega}{\omega_0}\right) + \left[\frac{1+u^2\sec^2\theta}{2u\sec\theta}\right]^2 \sin^2\left(n\pi\frac{\omega}{\omega_0}\right)}, \tag{2}$$

$$\tau_{TM} = \frac{1}{\cos^2\left(n\pi\frac{\omega}{\omega_0}\right) + \left[\frac{\varepsilon^2+u^2\sec^2\theta}{2\varepsilon u\sec\theta}\right]^2 \sin^2\left(n\pi\frac{\omega}{\omega_0}\right)}. \tag{3}$$

Both functions are maximized at the frequencies $\omega = \frac{m}{n}\omega_0$ with $m \in \mathbb{N}^*$ by taking unitary value. In addition, they are

both minimized at $\omega = \frac{2m-1}{2n}\omega_0$ with $m \in \mathbb{N}^*$; their minimal values are given by $\tau_{TE} = \left[\frac{1+u^2\sec^2\theta}{2\,u\sec\theta}\right]^{-2}$ for TE waves and by $\tau_{TM} = \left[\frac{\varepsilon^2+u^2\sec^2\theta}{2\varepsilon u\sec\theta}\right]^{-2}$ for TM waves.

One may aim at using the simple setup of Fig. 1(a) for filtering electromagnetic waves by letting them pass at $\omega = \omega_0$ and blocking all the other frequencies within the range $\omega_1 < \omega < \omega_2$, as shown in the sketch of Fig. 1(b). In particular, we demand the transmissivity to diminish away from the passing frequency $\omega = \omega_0$ without increasing again; in other words, a strictly increasing behavior of $\tau_{TE/TM}(\omega)$ for $\omega_1 < \omega < \omega_0$ and a strictly decreasing one for $\omega_0 < \omega < \omega_2$ is requested. Indeed, the functions $\tau_{TE/TM}(\omega)$ are periodically oscillating with respect to ω (of period ω_0/n) between unity and their minimal values; our objective calls for a single maximum (at $\omega = \omega_0$) across the defined window $\omega_1 < \omega < \omega_2$, without the two neighboring ones being close to its respective limits for both polarizations. Such a goal is well served if the two minima of the transmissivities $\tau_{TE/TM}(\omega)$ for $m = n$ and $m = n+1$ appear outside of the specified band, namely [47]:

$$\left\{\omega_1 > \frac{2n-1}{2n}\omega_0\ ,\ \omega_2 < \frac{2n+1}{2n}\omega_0\right\} \Rightarrow n < \frac{1}{2\max\left\{1-\frac{\omega_1}{\omega_0}, \frac{\omega_2}{\omega_0}-1\right\}}, \quad (4)$$

while the maximum of $m = n$ occurs at $\omega = \omega_0$. It is straightforward to show that for $\omega_1/\omega_0 < 0.5$ or $\omega_2/\omega_0 > 1.5$, there is no positive integer n to satisfy (4) and thus the proposed inverse design approach fails. The described process can be considered as treatment to an inverse problem since one specifies the characteristic frequencies $\{\omega_1, \omega_0, \omega_2\}$ and the analytical formulas (1),(4) give optimal thicknesses for the Fabry-Perot resonator of fixed dispersion-less permittivity ε and at a constant incidence angle θ.

III. NUMERICAL RESULTS

A. RESIDUAL TRANSMISSIVITIES

The performance of the filter will be certainly related to the maximum residual transmissivities at the ends of the considered frequency interval, namely, the quantities $r_{TE/TM} = \max\{\tau_{TE/TM}(\omega_1), \tau_{TE/TM}(\omega_2)\}$, as indicated by Fig. 1(b). Indeed, the more successful the filtering, the more suppressed the transmission from the filters at the ends of the regarded band for both polarizations. Therefore, it would be meaningful to examine the variation of these two quantities, in order to judge under which conditions the sharpness of the proposed filter becomes substantial.

In Fig. 2(a), we show the trajectories of the device response on the map of residual transmissivities for both wave types (r_{TE}, r_{TM}) when the incidence direction varies from normal ($\theta = 0°$) to parallel ($\theta = 90°$) to the interface, for various Fabry-Perot orders n, given by the inequality (4). As long as the incoming rays meet the boundary normally ($\theta = 0°$), there is no difference between the two polarizations and that is

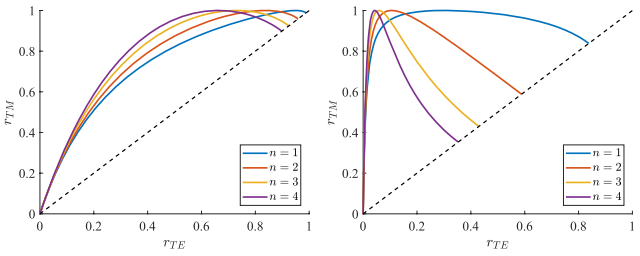

FIGURE 2. The residual transmissivities for both polarizations (r_{TE}, r_{TM}) as sweeping the incidence angle $0° < \theta < 90°$, for various Fabry-Perot orders n. Normal incidence ($\theta = 0°$) corresponds to the starting points from the dashed lines where $r_{TE} = r_{TM}$ and the two polarizations are identical; Grazing angle ($\theta = 90°$) corresponds to the ending point at the origin. (a) $\varepsilon = 2$, (b) $\varepsilon = 20$. Plot parameters: $\omega_1/\omega_0 = 0.9$, $\omega_2/\omega_0 = 1.1$. Each point of the curves corresponds to a different filter optimized for different angle θ and describing interference of different Fabry-Perot order n.

why the corresponding points exist along the dashed identity line $r_{TE} = r_{TM}$. Note that for $\theta = 0°$ the filter behaves more efficiently when the interference order is large, meaning that the best choice for n would be the maximal integer indicated by (4). Once the incident beam becomes more oblique, r_{TE} decreases and r_{TM} is maximized for specific angles before declining along with r_{TE}; apparently, both the quantities vanish for $\theta \to 90°$.

In Fig. 2(b), we repeat the same calculations but for a much denser dielectric (larger ε) and is clear that the spread between different-order trajectories enlarges. As a result, the filters are very effective when n is close to maximal. In addition, for higher n, the variation of both (r_{TE}, r_{TM}) is sharper with respect to θ since d increases and the incoming ray covers a larger path into the slab. It should be stressed that for each angle θ, the size of the layer d, changes according to (1) even at a fixed order n; therefore, every single point of the curves corresponds a different slab that has been optimized according to the proposed technique.

In Fig. 3(a), we represent the mean of the two residual transmissivities $r = \frac{r_{TE}+r_{TM}}{2}$ in dB as a function of the two frequencies $(\omega_1/\omega_0, \omega_2/\omega_0)$ that determine the operational band of the filter for the smallest possible d, namely at the fundamental resonance $n = 1$. One clearly notices the blank areas that correspond to infeasible combinations of frequencies preventing the condition (4) from being fulfilled. Furthermore, the isocontour levels have rectangular shape as imposed by the linear nature of the expressions at the arguments of max functions in (4). We finally notice that the efficiency of the filter is better for $\omega_1 \to \omega_0/2$ and $\omega_2 \to 3\omega_0/2$; such a specification considers the behavior of the system across a larger frequency range where resonant responses are possible with moderate thickness d. On the contrary, the filtering task becomes more challenging when $\omega_1 \to \omega_2$ since $n = 1$ and very sharp changes in $\tau(\omega)$ are ruled out; therefore, the performance r of the photonic filter deteriorates for increasing ω_1 and decreasing ω_2.

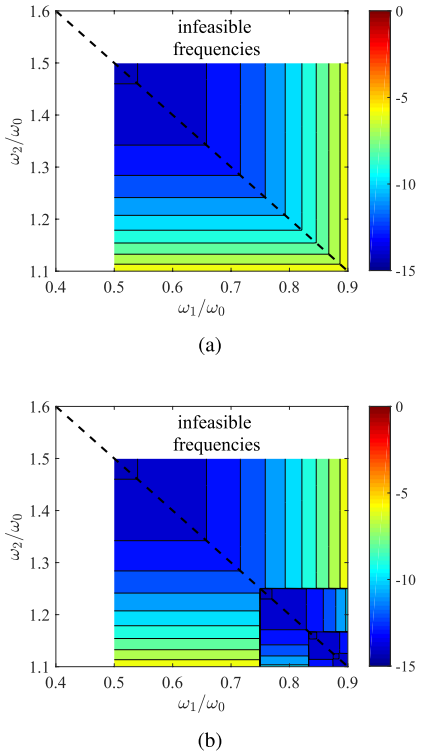

FIGURE 3. The average residual transmissivity $r = \frac{r_{TE}+r_{TM}}{2}$ in dB as function of the two frequencies $(\omega_1/\omega_0, \omega_2/\omega_0)$ defining the band of the photonic filter. (a) First Fabry-Perot order $n = 1$, (b) Maximum Fabry-Perot order n, according to (4). Plot parameters: $\varepsilon = 100$, $\theta = 0°$. The white regions indicate infeasible combinations of frequencies for which there is no optimal interference order $n \in \mathbb{N}$ able to satisfy the inverse design specifications. Each point of the contour plots corresponds to a different filter optimized for different frequency ranges.

In Fig. 3(b), we show the same quantity $r = r(\omega_1, \omega_2)$ as a function of the characteristic frequencies $(\omega_1/\omega_0, \omega_2/\omega_0)$ for the thicker optimal design, namely with the highest Fabry-Perot interference order n according to (4) (maximum thickness d). The discontinuous variation is apparently attributed to the change in the value of n as the limits of the operational band alter accordingly. It is noteworthy that the average residual transmissivity r drops significantly along the line $\omega_1 + \omega_2 = 2\omega_0$ of symmetric response, exhibiting a fractal-like variation on the considered map due to the jumps of n by unity. However, for most of the combinations (ω_1, ω_2) the only permitted order for the developed Fabry-Perot interference is the fundamental $n = 1$ and thus the represented quantity r is identical to that of Fig. 3(a); the same happens for the infeasibility parametric region.

In Fig. 4, we examine the effect of the incidence angle θ and the ratio of the characteristic frequencies ω_1/ω_2 with a centralized filtering frequency $\omega_0 = \frac{\omega_1+\omega_2}{2}$ on the residual transmissivities $\{r_{TE}, r_{TM}\}$; the resonance order n is taken equal to maximum from (4). In Fig. 4(a), we consider the TE waves and realize that the average values are quite small indicating highly selective functionality and further decrease when the incoming ray gets more and more oblique.

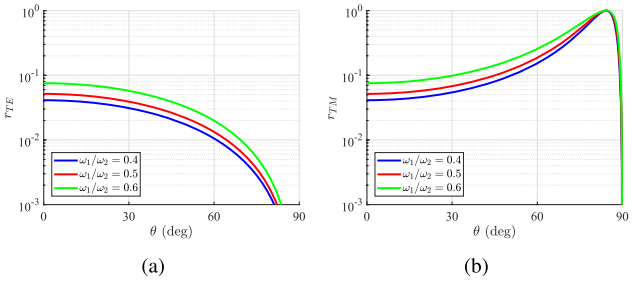

FIGURE 4. The residual transmissivities as functions of incidence angle θ for various frequency ratios ω_1/ω_2 with $\omega_0 = \frac{\omega_1+\omega_2}{2}$. (a) r_{TE}, (a) r_{TM}. Plot parameters: $\varepsilon = 100$, maximum Fabry-Perot order n. Each point of the curves corresponds to a different filter optimized for different angle θ and frequency ratio ω_1/ω_2.

In Fig. 4(b), TM polarization is regarded and the opposite trend with respect to θ is recorded before the well-known rapid drop near the grazing angle ($\theta \to 90°$). Such a difference between the two polarizations of waves is attributed to the fact that the deployed material is dielectric but non-magnetic; once θ increases, the TE wave participates at the boundary conditions with its entire electric field; on the contrary, the TM wave concerns only the tangential electric component which vanishes for $\theta \to 90°$. In addition, the larger is the frequency ratio ω_1/ω_2, the worst the filter is since the design gets more demanding; the same happens in Fig. 4(a).

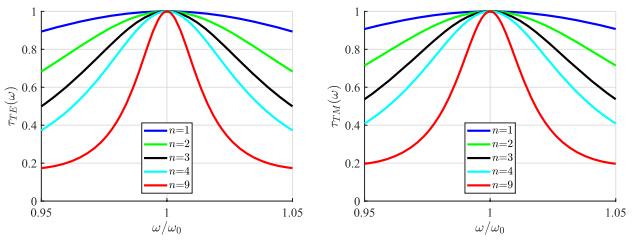

FIGURE 5. Frequency response of optimal filters corresponding to various Fabry-Perot orders of resonance n. Plot parameters: $\varepsilon = 20$, $\theta = 50°$. (a) TE waves, (b) TM waves. Each pair of curves in the two graphs corresponds to a single filter of different thickness d.

B. FILTERS FREQUENCY RESPONSE

Having understood the significance of the frequency range on the performance of the filter, the beneficial effect of Fabry-Perot interference order n on the selectivity of the device for both the incoming polarizations and the trade-off between the two when the incidence angle changes, it would be meaningful to show certain frequency responses. In Fig. 5, we show the transmissivities as functions of ω for various thicknesses d of the slab corresponding to different orders n from (4). By inspection of Fig. 5(a), one clearly recognizes the higher filtering efficiency once n increases in the presence of TE waves; similar findings are reported for TM illumination in Fig. 5(b), but, due to the dielectric

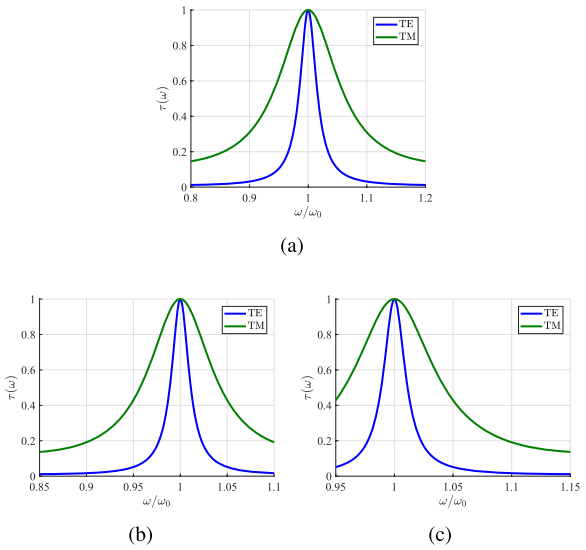

FIGURE 6. The transmissivity of the filter $\tau(\omega)$ as function of the normalized harmonic frequency ω/ω_0 for both polarizations (TE/TM). **(a)** $\omega_1/\omega_0 = 0.8$, $\omega_2/\omega_0 = 1.2$. **(b)** $\omega_1/\omega_0 = 0.85$, $\omega_2/\omega_0 = 1.1$. **(c)** $\omega_1/\omega_0 = 0.95$, $\omega_2/\omega_0 = 1.15$. Plot parameters: $\varepsilon = 100$, $\theta = 45°$. All points of the curves correspond to the same filter.

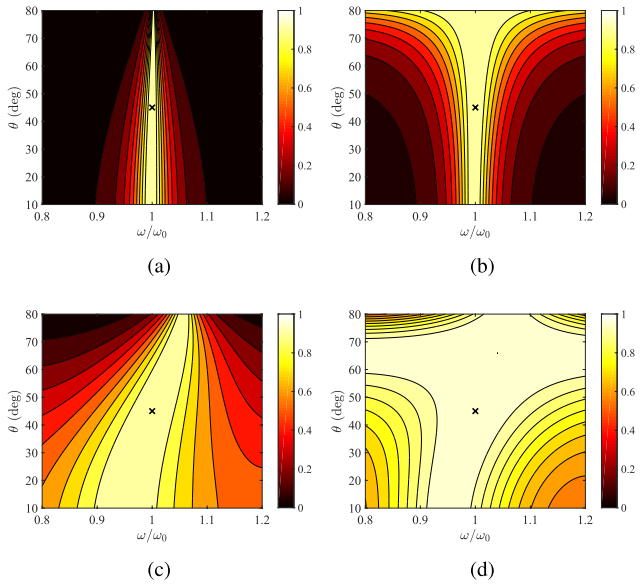

FIGURE 7. The transmissivities for both polarizations (TE/TM) of the filter τ represented in contour plot with respect to operational frequency ω/ω_0 and incidence angle θ. **(a,b)** $\varepsilon = 100$, **(c,d)** $\varepsilon = 5$. **(a,c)** $\tau_{TE}(\omega, \theta)$, **(a,c)** $\tau_{TM}(\omega, \theta)$. The first pair of contours (a,b) corresponds to one filter and the second pair (c,d) to another filter. The symbols × signify the optimal operation points.

nature of the material ($\varepsilon > 1$), the performance is slightly poorer ($r_{TM} > r_{TE}$).

This difference in the selectivity of TE and TM waves is also demonstrated by Fig. 6 where a much denser lossless dielectric medium is utilized ($\varepsilon = 100$) and excited by obliquely incident ($\theta = 45°$) waves. In Fig. 6(a), a symmetric response is required, while in Figs 6(b),6(c) the maxima are chosen to appear at positions of lower or higher oscillation frequencies respectively. One directly notes that the curves are identical in all the three panels of Fig. 6; the only feature that varies are the minima and the maxima of the working band $\omega_1 < \omega < \omega_2$. Inevitably, when we move from the condition $\omega_0 = \frac{\omega_1+\omega_2}{2}$, the residual transmissivities (r_{TE}, r_{TM}) increase and the filtering performance of our setup deteriorates.

In Fig. 7, we represent the transmissivities of the considered slab on the plane of the two spectra: frequency (ω/ω_0) and angular (θ); the systems are optimized for $\theta = 45°$. In the first two Figs 7(a),7(b), we assume a dense dielectric ($\varepsilon = 100$) and thus notice that both transmissivities τ_{TE} (Fig. 7(a)) and τ_{TM} (Fig. 7(b)) are almost symmetric, regardless of the incidence angle. Indeed, $u(\theta) = \sqrt{\varepsilon - \sin^2\theta} \cong \sqrt{\varepsilon}$, is practically independent from θ when $\varepsilon \gg 1$. Impressively, the variation of $\tau_{TE}(\omega)$ becomes sharper once the angle θ increases, even though the structure is designed for one direction; as far as the TM waves are concerned, the filtering performance worsens with θ.

In Figs 7(c),7(d), we repeat the calculations of Figs 7(a),7(b) but by deploying a much sparser material ($\varepsilon = 5$). The frequency response of the filter is symmetric only at the pre-selected angle $\theta = 45°$ while gets significantly distorted away from it. Interestingly, the proposed layer for very oblique TE rays (Fig. 7(c)) keeps exhibiting a sharper transmissivity, as happening in Fig. 7(a); on the contrary, the transmissivity spectrum for TM fields (Fig. 7(d)) flattens completely for a large cone of incident beams.

It should be stressed that this study presents the limits for filtering operation of a very simple setup (Fig. 1(a)), under the assumption that a dense dispersion-less dielectric with almost negligible losses ($\mathrm{Re}[\varepsilon] \gg |\mathrm{Im}[\varepsilon]|$) is available. Therefore, the functionality of the described concept is restricted to low sub-terahertz photonic frequencies ω, where losses of insulators are suppressed and their permittivities ε are rather non-dispersive [48].

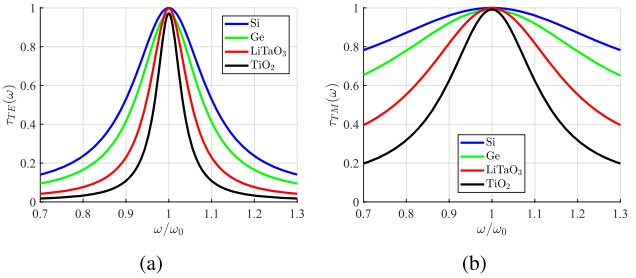

FIGURE 8. The transmissivity $\tau_{TE/TM}(\omega)$ of optimal Fabry-Perot filters as function of the normalized harmonic frequency ω/ω_0 for various employed media operated at sub-terahertz frequencies (silicon, germanium, lithium tantalate, titania). **(a)** TE fields, **(b)** TM fields. $\theta \cong 58°$.

In Fig. 8, we represent the transmissivity for both polarizations as a function of oscillating frequency ω for various employed media (silicon, germanium, lithium tantalate, titania). In Fig. 8(a), where TE waves are considered, we observe sharp maximizations for a quite extended operational band

($0.7\omega_0 < \omega < 1.3\omega_0$). Obviously, as indicated by Fig. 7, the larger is the real part of the permittivity $\mathrm{Re}[\varepsilon]$, the more selective the filtering is and thus TiO_2 Fabry-Perot resonator with its $\mathrm{Re}[\varepsilon] \cong 96$, does a much better job than the Si-based design ($\mathrm{Re}[\varepsilon] \cong 12$). As far as the imaginary part of the permittivity $\mathrm{Im}[\varepsilon]$ is concerned, one directly understands its harming influence on the transmissivity at $\omega = \omega_0$, which is not anymore perfect, especially for Ge ($\mathrm{Im}[\varepsilon] \cong -0.04$) and TiO_2 ($\mathrm{Im}[\varepsilon] \cong -0.1$). Indeed, even a so moderate $|\mathrm{Im}[\varepsilon]|$ is responsible for non-negligible absorption, let alone larger losses at higher frequencies ω (infrared, visible or ultraviolet).

In Fig. 8(b), we assume TM illumination and the sharpness of the depicted resonances is much weaker compared to TE case, as also suggested by Fig. 6. As indicated above, such a finding is due to the fact that our samples are non-magnetic; thus, it cannot support large magnetic flux density within its volume with substantial contrast. On the other hand, electric flux density difference inside and outside the slab can be very high (due to large ε) and it is exactly this property that inherits significant selectivity for TE waves. Nonetheless, it can be seen from Fig. 8(b) that significant ε contributes also to the filtering sharpness for TM signals.

IV. CONCLUSION

Many schemes, algorithms and recipes have been formulated for the design of electronic filters during the previous century. However, only recently an increased scientific interest has been recorded for photonic filtering of electromagnetic fields. The simplest mechanism that is utilized in frequency selection of optical waves regardless of their polarization, are the so-called Fabry-Perot interferences between pulses propagating along different directions. We optimally engineer these resonances so that a single dielectric slab transmits 100% at a specific frequency and suppresses the rest of waves within a considered band, for both polarizations. The reported results serve the purpose of inverse design that is currently attracting huge attention; indeed, analytical formulas are provided for the thickness and texture of the layer combined with suitable angle of incidence so that the filtering job is compatible with the specifications. Under certain conditions, like dense dielectrics and sufficiently narrow bands, the sharpness of the optimal filters has been found substantial and therefore the provided inverse-design expressions have been proven successful.

An interesting expansion of the present work would be to consider several dielectric layers of different materials making a more complex filter whose transmissivity would be predetermined at multiple frequencies. Such a multi-parametric configuration will support more enriched wave dynamics through its response and enable tunable filtering operations. However, the inverse design and the involving optimizations will not be anymore susceptible to analytical treatment; instead, state-of-the-art fast techniques like those incorporating gradient-based methods and deep-learning algorithms would be required.

REFERENCES

[1] G. Matthaei, E. M. T. Jones, and L. Young, *Microwave Filters, Impedance-Matching Networks, and Coupling Structures*. Norwood, MA, USA: Artech House, 1985, pp. 49–83.

[2] A. Fettweis, "Wave digital filters: Theory and practice," *Proc. IEEE*, vol. 74, no. 2, pp. 270–327, Feb. 1986, doi: 10.1109/PROC.1986.13458.

[3] M. Makimoto and S. Yamashita, "Bandpass filters using parallel coupled stripline stepped impedance resonators," *IEEE Trans. Microw. Theory Techn.*, vol. 28, no. 12, pp. 1413–1417, Dec. 1980, doi: 10.1109/TMTT.1980.1130258.

[4] W. T. Freeman and E. H. Adelson, "The design and use of steerable filters," *IEEE Trans. Pattern Anal. Mach. Intell.*, vol. 13, no. 9, pp. 891–906, Sep. 1991, doi: 10.1109/34.93808.

[5] M. Liserre, F. Blaabjerg, and S. Hansen, "Design and control of an LCL-filter-based three-phase active rectifier," *IEEE Trans. Ind. Appl.*, vol. 41, no. 5, pp. 1281–1291, Sep. 2005, doi: 10.1109/TIA.2005.853373.

[6] J. Capmany, B. Ortega, and D. Pastor, "A tutorial on microwave photonic filters," *J. Lightw. Technol.*, vol. 24, no. 1, pp. 201–229, Jan. 2006, doi: 10.1109/JLT.2005.860478.

[7] V. R. Almeida, C. A. Barrios, R. R. Panepucci, and M. Lipson, "All-optical control of light on a silicon chip," *Nature*, vol. 431, no. 7012, pp. 1081–1084, Oct. 2004, doi: 10.1038/nature02921.

[8] S. Savoia, G. Castaldi, V. Galdi, A. Alù, and N. Engheta, "Tunneling of obliquely incident waves through PT-symmetric epsilon-near-zero bilayers," *Phys. Rev. B, Condens. Matter*, vol. 89, no. 8, Feb. 2014, Art. no. 085105, doi: 10.1103/PhysRevB.89.085105.

[9] Y. Shen, D. Ye, I. Celanovic, S. G. Johnson, J. D. Joannopoulos, and M. Solja I, "Optical broadband angular selectivity," *Science*, vol. 343, no. 6178, pp. 1499–1501, Mar. 2014, doi: 10.1126/science.1249799.

[10] R. Dorn, S. Quabis, and G. Leuchs, "Sharper focus for a radially polarized light beam," *Phys. Rev. Lett.*, vol. 91, no. 23, Dec. 2003, Art. no. 233901, doi: 10.1103/PhysRevLett.91.233901.

[11] H. T. Miyazaki and Y. Kurokawa, "Squeezing visible light waves into a 3-nm-thick and 55-nm-long plasmon cavity," *Phys. Rev. Lett.*, vol. 96, no. 9, Mar. 2006, doi: 10.1103/PhysRevLett.96.097401.

[12] R. A. Minasian, "Photonic signal processing of microwave signals," *IEEE Trans. Microw. Theory Techn.*, vol. 54, no. 2, pp. 832–846, Feb. 2006, doi: 10.1109/TMTT.2005.863060.

[13] D. J. Masiello, and L. He, *DMREF: Collaborative Research: Nanoscale Temperature Manipulation via Plasmonic Fano Interferences, NSF Award 1727092*. Seattle, WA, USA: Univ. of Washington, Jul. 2017.

[14] B. Mattis and M. Nair, *SBIR Phase II: 3D Photonic Filters for Full Duplex, Interference Free Network Links, NSF Award 1926684*. Austin, TX, USA: GenXComm Inc., Sep. 2019.

[15] J. M. Vaughan, *The Fabry-Pérot Interferometer: History, Theory, Practice and Applications*. New York, NY, USA: Taylor & Francis, 1989, pp. 100–154.

[16] A. G. Fox and T. Li, "Resonant modes in a maser interferometer," *Bell Syst. Tech. J.*, vol. 40, no. 2, pp. 453–488, Mar. 1961, doi: 10.1002/j.1538-7305.1961.tb01625.x.

[17] W. Liang, M. Bockrath, D. Bozovic, J. H. Hafner, M. Tinkham, and H. Park, "Fabry–Pérot interference in a nanotube electron waveguide," *Nature*, vol. 411, no. 6838, pp. 665–669, Jun. 2001, doi: 10.1038/35079517.

[18] A. D. Kersey, T. A. Berkoff, and W. W. Morey, "Multiplexed fiber Bragg grating strain-sensor system with a fiber Fabry–Pérot wavelength filter," *Opt. Lett.*, vol. 18, no. 16, pp. 1370–1372, Aug. 1993, doi: 10.1364/OL.18.001370.

[19] M. Furchi, A. Urich, A. Pospischil, G. Lilley, K. Unterrainer, H. Detz, P. Klang, A. M. Andrews, W. Schrenk, G. Strasser, and T. Mueller, "Microcavity-integrated graphene photodetector," *Nano Lett.*, vol. 12, no. 6, pp. 2773–2777, May 2012, doi: 10.1021/nl204512x.

[20] B. H. Lee, Y. H. Kim, K. S. Park, J. B. Eom, M. J. Kim, B. S. Rho, and H. Y. Choi, "Interferometric fiber optic sensors," *Sensors*, vol. 12, no. 3, pp. 2467–2486, Feb. 2012, doi: 10.3390/s120302467.

[21] M. A. Kats, R. Blanchard, P. Genevet, and F. Capasso, "Nanometre optical coatings based on strong interference effects in highly absorbing media," *Nature Mater.*, vol. 12, no. 1, pp. 20–24, Jan. 2013, doi: 10.1038/NMAT3443.

[22] Z. Wang, X. Wang, S. Cong, J. Chen, H. Sun, Z. Chen, G. Song, F. Geng, Q. Chen, and Z. Zhao, "Towards full-colour tunability of inorganic electrochromic devices using ultracompact Fabry–Pérot nanocavities," *Nature Commun.*, vol. 11, no. 1, Jan. 2020, Art. no. 302, doi: 10.1038/s41467-019-14194-y.

[23] F. Capasso, K. Mohammed, and A. Cho, "Resonant tunneling through double barriers, perpendicular quantum transport phenomena in superlattices, and their device applications," *IEEE J. Quantum Electron.*, vol. 22, no. 9, pp. 1853–1869, Sep. 1986, doi: 10.1109/JQE.1986.1073171.

[24] C. Valagiannopoulos, "Quantum Fabry–Pérot resonator: Extreme angular selectivity in matter-wave tunneling," *Phys. Rev. A, Gen. Phys.*, vol. 12, no. 5, Nov. 2019, doi: 10.1103/PhysRevApplied.12.054042.

[25] C. Valagiannopoulos, "Predicting the quantum texture from transmission probabilities," *J. Appl. Phys.*, vol. 127, no. 17, May 2020, Art. no. 174301, doi: 10.1063/5.0006780.

[26] P. Morris, A. Hurrell, A. Shaw, E. Zhang, and P. Beard, "A Fabry–Pérot fiber-optic ultrasonic hydrophone for the simultaneous measurement of temperature and acoustic pressure," *J. Acoust. Soc. Amer.*, vol. 125, no. 6, pp. 3611–3622, Jun. 2009, doi: 10.1121/1.3117437.

[27] G. Wild and S. Hinckley, "Acousto-ultrasonic optical fiber sensors: Overview and state-of-the-art," *IEEE Sensors J.*, vol. 8, no. 7, pp. 1184–1193, Jul. 2008, doi: 10.1109/JSEN.2008.926894.

[28] T. J. Kippenberg, H. Rokhsari, T. Carmon, A. Scherer, and K. J. Vahala, "Analysis of radiation-pressure induced mechanical oscillation of an optical microcavity," *Phys. Rev. Lett.*, vol. 95, no. 3, Jul. 2005, doi: 10.1103/PhysRevLett.95.033901.

[29] F. Xu, D. Ren, X. Shi, C. Li, W. Lu, L. Lu, L. Lu, and B. Yu, "High-sensitivity Fabry–Pérot interferometric pressure sensor based on a nanothick silver diaphragm," *Opt. Lett.*, vol. 37, no. 2, pp. 133–135, Jan. 2012, doi: 10.1364/OL.37.000133.

[30] M. J. Hartmann and M. B. Plenio, "Steady state entanglement in the mechanical vibrations of two dielectric membranes," *Phys. Rev. Lett.*, vol. 101, no. 20, Nov. 2008, doi: 10.1103/PhysRevLett.101.200503.

[31] K. Seshan, *Handbook of Thin Film Deposition Processes and Techniques*. Norwich, NY, USA: Noyes, 2001, pp. 45–149.

[32] Y. Wang, X. Zhu, Y. Chen, H. Shi, Z. Li, S. Zhang, Q. Liu, Y. Li, Q. Xiang, and H. Duan, "Fabrication of Fabry–Pérot-cavity-based monolithic full-color filter arrays using a template-confined micro-reflow process," *J. Micromech. Microeng.*, vol. 29, no. 2, Feb. 2019, Art. no. 025008, doi: 10.1088/1361-6439/aaf6cb.

[33] Z. Li, S. Butun, and K. Aydin, "Large-area, lithography-free super absorbers and color filters at visible frequencies using ultrathin metallic films," *ACS Photon.*, vol. 2, no. 2, pp. 183–188, Feb. 2015, doi: 10.1021/ph500410u.

[34] Y.-J. Rao, M. Deng, D.-W. Duan, X.-C. Yang, T. Zhu, and G.-H. Cheng, "Micro Fabry–Pérot interferometers in silica fibers machined by femtosecond laser," *Opt. Express*, vol. 15, no. 21, pp. 14123–14128, Oct. 2007, doi: 10.1364/OE.15.014123.

[35] T. C. L. G. Sollner, P. E. Tannenwald, D. D. Peck, and W. D. Goodhue, "Quantum well oscillators," *Appl. Phys. Lett.*, vol. 45, no. 12, pp. 1319–1321, Dec. 1984, doi: 10.1063/1.95134.

[36] G. Lu and J. T. Hupp, "Metal–organic frameworks as sensors: A ZIF-8 based Fabry–Pérot device as a selective sensor for chemical vapors and gases," *J. Amer. Chem. Soc.*, vol. 132, no. 23, pp. 7832–7833, Jun. 2010, doi: 10.1021/ja101415b.

[37] L. R. Pendergrass and R. S. Rogowski, *Fabrication of Fabry–Pérot Interferometer Sensors and Characterization of Their Performances for Aircraft Inspection*, NASA Langley Res. Center, Hampton, VA, USA, 1995, pp. 579–588.

[38] J. S. Patel and S. Lee, "Electrically tunable and polarization insensitive Fabry–Perot étalon with a liquid-crystal film," *Appl. Phys. Lett.*, vol. 58, no. 22, pp. 2491–2493, Jun. 1991, doi: 10.1063/1.104853.

[39] O. D. Miller, "Photonic design: From fundamental solar cell physics to computational inverse design," Ph.D. dissertation, Dept. Elect. Eng. Comput. Sci., Univ. California, Berkeley, CA, USA, 2013, pp. 61–101.

[40] S. Molesky, Z. Lin, A. Y. Piggott, W. Jin, J. Vučković, and A. W. Rodriguez, "Inverse design in nanophotonics," *Nature Photon.*, vol. 12, no. 11, pp. 659–670, Nov. 2018, doi: 10.1038/s41566-018-0246-9.

[41] J. Peurifoy, Y. Shen, L. Jing, Y. Yang, F. Cano-Renteria, B. G. DeLacy, J. D. Joannopoulos, M. Tegmark, and M. Soljačić, "Nanophotonic particle simulation and inverse design using artificial neural networks," *Sci. Adv.*, vol. 4, no. 6, Jun. 2018, Art. no. eaar4206, doi: 10.1126/sciadv.aar4206.

[42] N. Mohammadi Estakhri, B. Edwards, and N. Engheta, "Inverse-designed metastructures that solve equations," *Science*, vol. 363, no. 6433, pp. 1333–1338, Mar. 2019, doi: 10.1126/science.aaw2498.

[43] C. Valagiannopoulos, "Photonic inverse design of simple particles with realistic losses in the visible frequency range," *Photonics*, vol. 6, no. 1, p. 23, Feb. 2019, doi: 10.3390/photonics6010023.

[44] Z. Lin, B. Groever, F. Capasso, A. W. Rodriguez, and M. Lončar, "Topology-optimized multilayered metaoptics," *Phys. Rev. A, Gen. Phys.*, vol. 9, no. 4, Apr. 2018,Art. no. 044030, doi: 10.1103/PhysRevApplied.9.044030.

[45] C. A. Valagiannopoulos, "A novel methodology for estimating the permittivity of a specimen rod at low radio frequencies," *J. Electromagn. Waves Appl.*, vol. 24, nos. 5–6, pp. 631–640, Apr. 2012, doi: 10.1163/156939310791036331.

[46] C. A. Valagiannopoulos, "On measuring the permittivity tensor of an anisotropic material from the transmission coefficients," *Prog. Electromagn. Res. B*, vol. 9, pp. 105–116, 2008, doi: 10.2528/PIERB08072005.

[47] C. Valagiannopoulos, "Optimally sharp energy filtering of quantum particles via homogeneous planar inclusions," *Sci. Rep.*, vol. 10, no. 1, Jan. 2020, Art. no. 816, doi: 10.1038/s41598-019-56793-1.

[48] A. Karalis, J. D. Joannopoulos, and M. Soljacic, "Efficient wireless non-radiative mid-range energy transfer," *Ann. Phys.*, vol. 323, pp. 34–48, Jan. 2008, doi: 10.1016/j.aop.2007.04.017.

CONSTANTINOS VALAGIANNOPOULOS (Senior Member, IEEE) was born in Athens, Greece, in 1982. He received the Dipl.Eng. degree (Hons.) in electrical engineering from the National Technical University of Athens, Greece, in 2004, and the Ph.D. degree in electromagnetic theory from the National Technical University of Athens, in 2009.

From 2010 to 2014, he was a Postdoctoral Researcher with the Group of Theoretical and Applied Electromagnetics of Complex Media, Department of Electronics and Nanoengineering, Aalto University, Finland, advised by Sergei Tretyakov. From 2014 to 2015, he was with the Laboratory of Metamaterials and Plasmonics, Department of Electrical and Computer Engineering, The University of Texas at Austin, TX, USA, advised by Andrea Alù. Since 2015, he has been with Nazarbayev University (NU), Kazakhstan, as an Assistant Professor, where he has also been an Associate Professor with the Department of Physics, since 2018. He leads the Metamaterials Modeling and Design Group, NU, where he performs research on the forward and inverse design of photonic devices manipulating the light and on the translation of electromagnetic concepts into quantum systems. He has authored or coauthored more than 100 works published at international refereed scientific journals and presented numerous reports in scientific conferences. He is currently participating as a Principal Investigator (PI) or co-PI in the successful execution of national and international research grants with total annual budget more than 600K USD.

Dr. Valagiannopoulos is a Senior Member of OSA, and was a recipient of the inaugural 2015 JOPT Research Excellence Award for his work: "Perfect absorption in graphene multilayers." He was Guest Editor of *Photonics* (MDPI) for the special issue including selected articles presented at 2019 Metamaterials Congress. He also received the International Chorafas Prize for the Best Doctoral Thesis, in 2008, the Academy of Finland Postdoctoral Grant for 2012—2015. Finally, he is the winner of the 2020 NU Teaching Award for Integrating Research and Teaching.